Formation of Deprotected Fuzzy Blobs in Chemically Amplified Resists

RONALD L. JONES,[1] TENGJIAO HU,[1] ERIC K. LIN,[1] WEN-LI WU,[1] DARIO L. GOLDFARB,[2] MARIE ANGELOPOULOS,[2] BRIAN C. TRINQUE,[3] GERARD M. SCHMID,[4] MICHAEL D. STEWART,[4] C. GRANT WILLSON[3,4]

[1]Polymers Division, National Institute of Standards and Technology, Gaithersburg, Maryland 20899

[2]IBM T. J. Watson Research Center, Yorktown Heights, New York 10598

[3]Department of Chemistry, University of Texas at Austin, Austin, Texas 78712

[4]Department of Chemical Engineering, University of Texas at Austin, Austin, Texas 78712

Received 31 October 2003; accepted 30 January 2004
DOI: 10.1002/polb.20168
Published online in Wiley InterScience (www.interscience.wiley.com).

ABSTRACT: The requirement of nanometer dimensional control in photolithographic patterning underlies the future of emerging technologies, including next-generation semiconductors, nanofluids, photonics, and microelectromechanical systems. For chemically amplified resists, dimensional control is mediated by the diffusion and reaction of photogenerated acids within a polymer-based photoresist matrix. The complex nature of the combined processes of reaction and diffusion prohibit the routine measurement of this phenomenon. Using small-angle neutron scattering, we have measured the form of the diffusion–reaction path of a photogenerated acid within a model photoresist matrix with a labeled protection group on the polymer side group. During the deprotection reaction, changes in the scattering form factor result from the shape and form of the deprotected regions. The individual volumes or blobs of reacted material are diffuse, with a fuzzy boundary between the reacted and unreacted regions. The impact of these results on the pattern quality is also discussed. © 2004 Wiley Periodicals, Inc.* J Polym Sci Part B: Polym Phys 42: 3063–3069, 2004
Keywords: micropatterning; photolithography; reaction diffusion; small-angle neutron scattering; photoresists; morphology; nanotechnology

INTRODUCTION

The reduction of sidewall roughness, a surface roughness found on the sides of patterns created in photoresists, is a critical requirement for further reductions in future microelectronic circuit dimensions. For the current technology node of optical lithography, required pattern widths of approximately 100 nm are produced with typical sidewall roughness of 1–3 nm. However, the drive to produce components with dimensions of approximately 30 nm or less will require control of the pattern dimensions to subnanometer levels.[1] Controlling the roughness to this level will in turn require a fundamental understanding of the mechanisms of sidewall roughness formation. For the most widely used class of photoresists, chemically amplified resists (CARs), a patterned image

Correspondence to: R. L. Jones (E-mail: ronald.jones@nist.gov)

Journal of Polymer Science: Part B: Polymer Physics, Vol. 42, 3063–3069 (2004)
© 2004 Wiley Periodicals, Inc. *This article is a US Government work and, as such, is in the public domain in the United States of America.

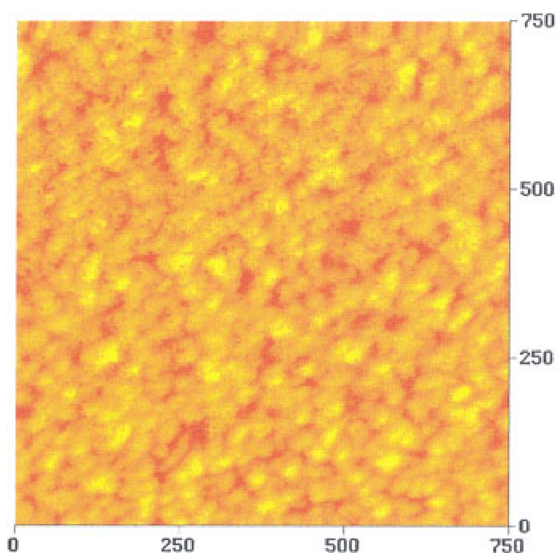

Figure 1. Atomic force microscopy topological image of a model sidewall surface created by the development of a PBOCSt film with a gradient in the deprotection at the surface. The rms roughness is approximately 2.5 nm. The lateral distances are in nanometers.

is recorded in a polymer-based photoresist with a photosensitive small molecule, a photoacid generator (PAG), that generates an acid upon exposure to ultraviolet light. During a subsequent postexposure bake (PEB), the acid catalyzes a deprotection reaction on the side chains of the polymer matrix, replacing hydrophobic side groups with hydrophilic moieties. Upon reaction, the acid regenerates and can diffuse to another reaction site. This regeneration has been reported to occur hundreds of times. In this manner, the photosensitive acids chemically amplify the patterned exposure of the ultraviolet light and cause imaged regions to selectively dissolve in an aqueous base developer solution. The resulting sidewall possesses a nodular morphology shown in Figure 1.

Current theories of pattern formation in photoresists typically include the formation of deprotected volumes by individual acids.[2–9] In current imaging systems, the spatial distribution and concentration of photogenerated acids are primarily controlled by the distribution of ultraviolet intensity at the edge of the patterned illumination.[2] The subsequent PEB, however, serves to fill in the gaps between acids as they each deprotect a volume of the polymer.[3–6] Over length scales larger than the paths of acid diffusion and reaction, these volumes overlap and determine the average solubility of the photoresist in the developer. Within the length scale of the deprotection volumes, however, the inhomogeneity created by the inherent distances between each acid is likely to create fluctuations in solubility and, therefore, in the local dissolution rate. At this level, which is theorized to be on the length scales of current sidewall roughness, the shape and distribution of deprotected regions could play a role in the creation of surface roughness.[5]

Schmid et al.[9] demonstrated through computer simulations, for CARs, the existence of an inhomogeneous distribution of deprotection. Using a Voronoi diagram, they suggested that the morphology of deprotection could be characterized as a collection of individual deprotection volumes created by individual acids. As illustrated in Figure 2, each acid possesses a sphere of influence within which the surrounding matrix solubility is transformed during PEB. Although typical loadings of PAGs in modern CARs are relatively small (ca. 1–5% mass fraction), the large fraction of acid-generated deprotection volumes created within the exposed region are clearly overlapped, and this results in a high dissolution rate. In contrast, the lack of exposure in the masked regions prevents significant deprotection in these areas, and any deprotection volumes are isolated. The pattern edge is formed at a gradient in the exposure dose; the final position of the

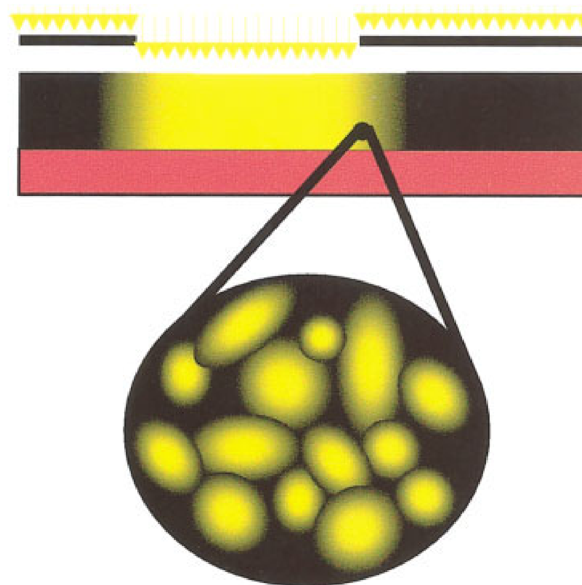

Figure 2. Schematic illustrating the patterned exposure (top) of a photoresist showing deprotected (light) and protected (dark) regions. The expanded image indicates the existence of fuzzy blobs of deprotection packed within a gradient in the deprotection at the edge of the patterned exposure.

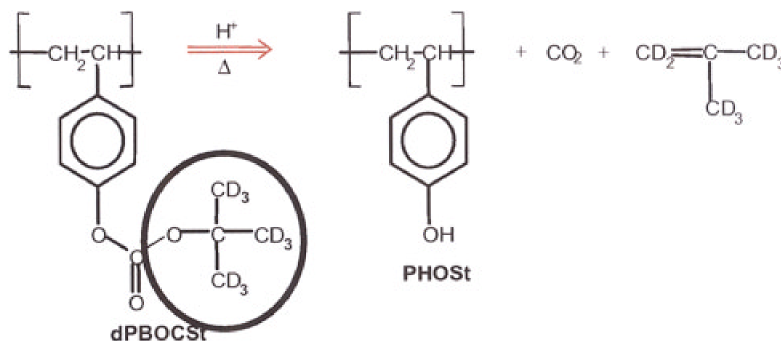

Figure 3. Schematic of the photoresist chemistry used in this study, including d-PBOCSt (left) with a pendant tert-butoxy carbonyloxy (*t*-BOC) group. After the generation of the small-molecule acid and subsequent PEB, the acid cleaves the *t*-BOC group, creating a series of volatile groups. Although the actual reaction is complex, it is typically approximated by the reaction shown, producing poly(hydroxystyrene) (PHOST) as a product of the reaction.

pattern sidewall within this gradient in the composition is determined by the strength of the developer. The pattern sidewall is then formed at a region of varying deprotection and varying dissolution rates. The morphology of deprotection is a likely parameter in determining the final sidewall morphology.

Evidence of deprotection morphology effects on the final sidewall roughness can be found in the work of He and Cerrina.[10] Atomic force microscopy of partially developed blanket-exposed films revealed a maximum in the root-mean-square (rms) roughness of the surface as a function of the exposure dose. Increases in the exposure dose result in an increased fraction of photogenerated acids in the films. The exposure dose, therefore, provides a manner of controlling the extent of deprotection. At the limits of zero and fully deprotected material, the morphology of deprotection in these films is characterized as homogeneous, and the resulting dissolution rate is likewise locally homogeneous. As the fraction of deprotection approaches an intermediate value, the morphology becomes increasingly inhomogeneous, and the rms roughness approaches a maximum. This observation has been previously explained with one-dimensional semiempirical models of dissolution rate based on the critical ionization model,[11] but the effects of morphology were not considered. Additional evidence of a connection between the deprotection morphology is demonstrated by the observation of increasing inhomogeneity in model sidewall morphology with increasing PEB time.[12–14]

In this article, we describe results from measurements of the deprotection volume created by dilute concentrations of acid molecules. In this case, the deprotection volumes created by each acid do not, on average, impinge on each other and represent the case of isolated deprotection regions. This limit is useful for determining the properties of individual deprotection volumes, including the shape and size, and provides insight into possible deprotection morphologies at sidewall interfaces. The deprotection volumes have been measured with small-angle neutron scattering (SANS) and represent the first known measurements of this phenomenon in a photoresist.

EXPERIMENTAL

Films of isotopically labeled poly(butoxy carbonyloxy styrene) (d-PBOCSt) with a PAG mass fraction of 0.7 ± 0.01% were spin-cast from solution in propylene glycol methyl ether acetate onto SEMI standard silicon wafers.[15] d-PBOCSt was synthesized[16] from poly(hydroxystyrene) through the substitution of di-*tert*-dicarbonate d18 ($M_{r,n}$ = 21000, where $M_{r,n}$ is the number average relative molecular mass, and polydispersity = 2.1). This synthesis reaction produced a poly(butoxy carbonyloxy styrene) (PBOCSt) backbone with isotopically labeled tertiary methyl side groups, as shown in Figure 3. The model PAG, di(*t*-butylphenyl)iodonium perfluorooctanesulfonate (PFOS), was obtained from Day Chem.[17] The d-PBOCSt/PFOS films were blanket-exposed to ultraviolet radiation from a broadband source ranging between 220 and 260 nm with a total dose of 500 mJ/cm^2. Each film was subsequently baked on a hotplate at 90 ± 1 °C for times ranging from 0 to 600 s. The

resulting level of deprotection was then determined as a function of the PEB time with Fourier transform infrared (FTIR) spectroscopy. Here, the extent of the reaction was determined via the monitoring of the carbonyl peak.[18] The relative scale of intensity was established by the measurement of a pure d-PBOCSt film and a pure poly(hydroxystyrene) film. The mass fraction of acid required to initiate measurable deprotection was determined to be approximately 0.5%. This level represents the minimum acid required to overcome contaminants present in the initial film. Contamination is known to play a significant role in the quenching of photogenerated acid, and experiments are typically performed in controlled atmospheres. Because the level of contamination is difficult to control precisely, we consider only the mass fraction of acid above the contamination level. This initial quantity of the photogenerated acid is, therefore, assumed to not significantly alter the resultant deprotection morphology. On the basis of the FTIR measurements, processing conditions were chosen to provide a significant level of deprotection (30 ± 5%) from a minimal concentration of acid (PFOS added mass fraction of 0.2 ± 0.01%). A set of 22 nominally identical films was cast and processed with a postapplication bake of 120 ± 1 °C for 300 ± 2 s with an exposure energy of 100 mJ/cm^2 and with PEB at 90 ± 1 °C for 120 ± 2 s. A second set of 22 films with no added PFOS was processed under the same conditions.

SANS measurements were performed at the National Institute of Standards and Technology Center for Neutron Research on the NG-1 8-m SANS beam line. To reduce background scattering, all windows were removed before the measurement between the sample and detector, and the sample chamber was subsequently evacuated of air. The samples were measured at room temperature, with an average measurement time of 12 h per sample. Initially, data were reduced through the subtraction of the background measured from a stack of 22 clean silicon substrates, with corrections for detector sensitivity and dark current contributions. The intensity was placed on an absolute scale through comparisons of the direct beam flux through the samples with that measured through a vacuum, and it was further normalized by a sample volume. The two-dimensional data were then circularly averaged. To extract the scattered intensity (I) due only to the path of deprotection, the intensity resulting from the protected samples (i.e., no added PFOS) was subtracted from that of the partially deprotected samples.

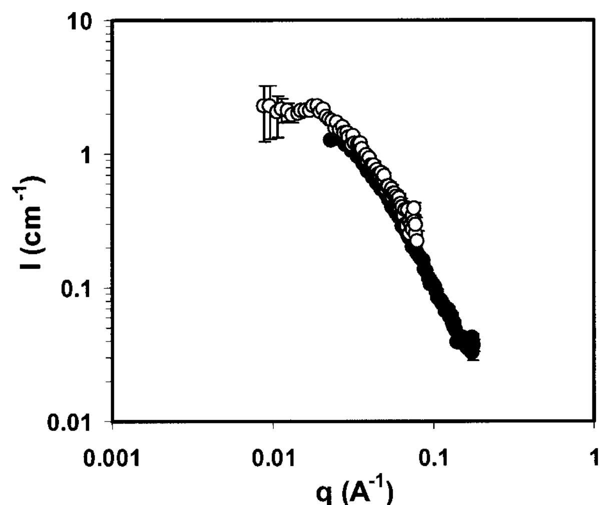

Figure 4. Data from SANS for a series of partially deprotected d-PBOCSt films. I is shown as a function of $\mathbf{q}$ on double logarithmic axes. Data from two configurations are merged as filled and open symbols.

RESULTS

In Figure 4, I from a partially deprotected d-PBOCSt sample is plotted as a function of the scattering vector ($\mathbf{q}$). The scaling of the data at high $\mathbf{q}$ values follows a power law of the form $I \sim \mathbf{q}^{-D_{\mathrm{f,deprot}}}$, where $D_{\mathrm{f,deprot}}$ is the fractal dimension of the deprotection path. A fit to the data over the range of $\mathbf{q} = 0.08-0.11$ Å^{-1} yields $D_{\mathrm{f,deprot}} = 2.2 \pm 0.4$. An ideal random walk possesses a fractal dimension of 2, and this indicates that the radius of the random walk volume grows as $N^{1/2}$, where N is the number of steps in the walk. In contrast, a compact, space-filling walk would scale as N. As with the random walk, the deprotection path does not fill space efficiently. As a result, the interior volume of the deprotection volume is inhomogeneous, with local areas of larger or smaller levels of deprotection. Although non-Gaussian distributions can also produce equivalent fractal dimensions, such as a Lorentzian, we cannot distinguish between these two distributions with the current SANS configuration and have chosen to approximate the distribution as a Gaussian form. Regardless of the precise distribution, the fractal dimension indicates that the deprotection volume is diffuse and not a homogeneous volume of deprotection.

The form of the deprotection volumes reflects isotropic diffusion. In contrast, a highly directed form of diffusion and reaction would result in a

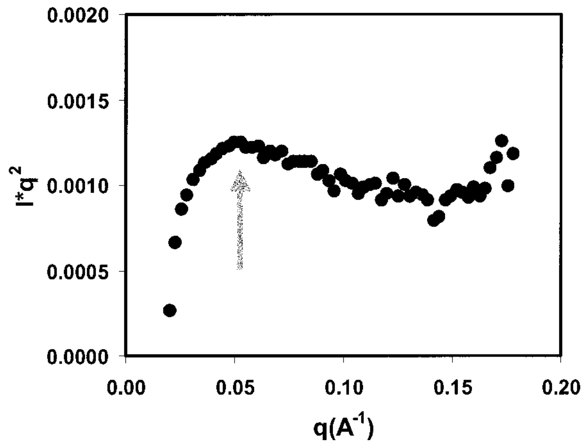

Figure 5. SANS data plotted in a Kratky form. $I\mathbf{q}^2$ is shown as a function of $\mathbf{q}$. Also shown is the onset of the Kratky asymptote at $\mathbf{q}R_G \approx 1$ (arrow).

lower fractal dimension, and a volume-filling reaction would result in a higher value. Although the diffusion–reaction mechanisms of photogenerated acids are known to be complex, with many side reactions and multiple volatile products,[19] the fractal dimension suggests that the path of deprotection is not significantly restricted by previously visited regions; this is analogous to the form of a polymer dissolved in a θ solvent. The deprotection path measured here quantifies the final path of deprotection only and cannot be used to separate the individual contributions of the diffusion and reaction of the acid. On the basis of these results, the average deprotection volume is characterized as a fuzzy blob, possessing a maximum in deprotection near the center that monotonically decays to the average protected composition of the initial resist matrix. The random walk scaling suggests the use of the Kratky limit to determine the average blob size through its radius of gyration ($R_{G,deprot}$). For a fractal dimension of 2, $I\mathbf{q}^2$ is a constant proportional to $R_{G,deprot}$ in the limit $\mathbf{q}R_{G,deprot} \gg 1$. The data at lower $\mathbf{q}$ values in Figure 5 follow a typical Kratky form. Data in the region $\mathbf{q} > 0.06$ Å^{-1} suffer from an overestimation of the background subtraction, and this makes a precise determination of $R_{G,deprot}$ difficult. Using the $\mathbf{q}$ value of maximum $I\mathbf{q}^2$ indicated in Figure 5, we estimate $R_{G,deprot} = 11.1 \pm 3$ nm.

As described previously, a patterned sidewall is formed within a gradient in he deprotection fraction at the edge of the exposure pattern. On the basis of the aforementioned results, the sidewall can now be described as a collection of fuzzy blobs that pack together in a manner dependent on the initial concentration of acid generated upon exposure and on material factors controlling the size of the blobs. The acid distribution is controlled by PAG chemistry, optical imaging conditions, such as the initial PAG concentration, aerial image, and chromophore efficiency. Because the developer determines the composition of the final sidewall, the deprotection morphology is then determined by the relative packing and form of the blobs, governed by factors controlling acid diffusion and reaction, including the PEB temperature and time, the glass-transition temperature of the resist, the activation energy of the PAG, and the reaction efficiency.

Because the blobs are diffuse and not volume-filling, overlap of the blobs will not necessarily create a homogeneous level of deprotection across the sidewall. To characterize the degree of spatial inhomogeneity in the deprotection morphology, we extract a correlation length (ξ) from the SANS data. Here, ξ represents a distance of interaction of the deprotection path. In the limit of a completely homogeneous level of deprotection, ξ would approach zero. In contrast, a maximum in ξ is expected for a deprotection morphology with the maximum spatial fluctuation in deprotection. In the limit of nonoverlapping deprotection paths, ξ is approximately equal to the size of the deprotection volume and will not strongly depend on the PAG concentration. In Figure 6, the data are presented as the inverse intensity versus $\mathbf{q}^2$ and are fit to a line. ξ is obtained from the ratio of the slope and intercept ($\xi = 12 \pm 1$ nm). This value is

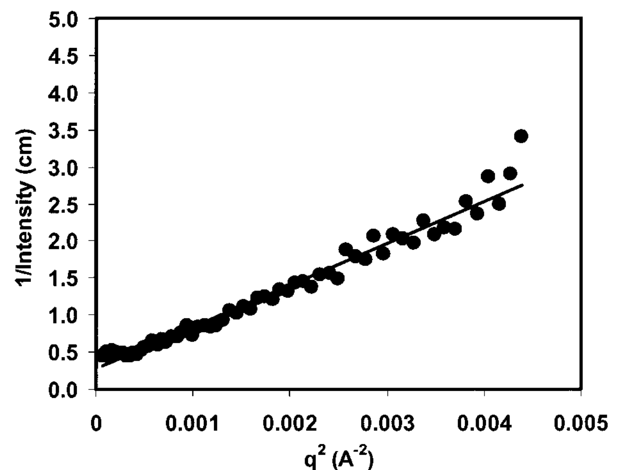

Figure 6. SANS data plotted as the inverse intensity versus $\mathbf{q}^2$. A linear fit (solid line) is used to extract ξ with a standard Ornstein–Zernicke analysis.

consistent with the average blob size obtained from the Kratky analysis and suggests that the characteristic length of inhomogeneity in the polymer matrix is that of the blob size.

This size scale can then be compared to the characteristic lengths found on model sidewalls.[12] On the basis of the form of the deprotection volume, we can calculate an effective diffusion–reaction coefficient of the acid. As an approximation, we assume the time to reach the PEB temperature is much smaller than the overall PEB time, and this allows the use of the PEB time as the time of acid diffusion. The random walk form suggests a simple Fickian representation in which $R_{G,deprot}$ is equal to $(2D_{deprot}t)^{0.5}$; t is 60 s, $R_{G,deprot}$ is 11 nm, and D_{deprot} is the diffusion–reaction coefficient for the acid. The resulting value of D_{deprot} ($\approx 1 \times 10^{-14}$ cm^2/s) is consistent with prior predictions based on experiments with the model bilayer. For an order-of-magnitude approximation of $R_{G,deprot}$ under different processing conditions, D_{deprot} is assumed to be relatively independent of temperature. Applying D_{deprot} to the conditions used in the bilayer (t = 90 s), we find that the predicted value of $R_{G,deprot}$ = 5 nm is consistent with estimates based on more extensive modeling in a different CAR. The size scale of the average deprotection volume associated with a single acid is, therefore, inconsistent with the length scales associated with observed model sidewall morphologies, for which the lateral length scales are approximately 5–6 $\times R_{G,deprot}$. Therefore, the surface of a sidewall cannot be simply described as a collection of impenetrable deprotection volumes. The larger size of the cutoff length scale could result from collections of overlapped blobs or possibly reflect the influence of the developer on the final morphology. Further description will require further insight into collective phenomena and phase behavior because of developer–resist interactions.

CONCLUSIONS

The form of the average deprotection volume created by individual acid molecules has been determined with SANS. The form is consistent with a simple random walk with an effective diffusion–reaction coefficient of approximately 1×10^{-14} cm^2/s. Within this volume, the level of deprotection is spatially inhomogeneous. On average, a maximum in deprotection occurs at the center of the volume, decaying to a background level at the edges. The volume is, therefore, described as a fuzzy blob. The interior of an imaged resist is considered as a distribution function of fuzzy blobs, in which the packing of the blobs determines the relative solubility in a developer solution. The final form of sidewall roughness is not consistent with a simple model of individual, noninteracting, and nonoverlapping fuzzy blobs, and this indicates the need for the further refinement of models describing the evolution of roughness at line edges and sidewalls of lithographically prepared structures.

This work was funded in part by the Defense Advanced Research Projects Agency (DARPA) Advanced Lithography Program under contract N66001-00-C-8083. Additional funding was provided by the National Institute of Standards and Technology Office of Microelectronics Programs. R. L. Jones is supported by a National Institute of Standards and Technology National Research Council postdoctoral fellowship.

REFERENCES AND NOTES

1. 2003 International Technology Roadmap. http://www.itrs.org; August 2003.
2. Houle, F. A.; Hinsberg, W. D.; Sanchez, M. I.; Hoffnagle, J. A. J Vac Sci Technol B 2002, 20, 924–931.
3. Cameron, J. F.; Ablaza, S. L.; Xu, G.; Yueh, W. Proc SPIE 1999, 3678, 785–799.
4. Patsis, G. P.; Tserepi, A.; Raptis, I.; Glezos, N.; Gogolides, E.; Valamontes, E. S. J Vac Sci Technol B 2000, 18, 3292–3295.
5. Yoshimura, T.; Shiraishi, H.; Yamamoto, J.; Okazaki, S. Appl Phys Lett 1993, 63, 764–768.
6. Yamaguchi, T.; Namatsu, H.; Nagase, M.; Yamazaki, K.; Kurihara, K. Appl Phys Lett 1997, 71, 2388–2390.
7. Dobisz, E.; Fedynyshyn, T. N.; Ma, D.; Shirey, L. M.; Bass, R. J Vac Sci Technol B 1998, 16, 3773–3778.
8. Hinsberg, W. D.; Houle, F. A.; Poliskie, G. M.; Pearson, D.; Sanchez, M. I.; Ito, H. J Phys Chem A 2002, 106, 9776–9787.
9. Schmid, G. M.; Smith, M. D.; Mack, C. A.; Singh, V. K.; Burns, S. D.; Willson, C. G. Proc SPIE 2000, 3999, 675–679.
10. He, D.; Cerrina, F. J Vac Sci Technol B 1998, 16, 3748–3751.
11. Tsiartas, P. C.; Flanagin, L. W.; Henderson, C. L.; Hinsberg, W. D.; Sanchez, I. C.; Bonnecaze, R. T.; Willson, C. G. Macromolecules 1997, 30, 4656–4664.
12. Jones, R. L.; Prabhu, V. M.; Goldfarb, D. L.; Lin, E. K.; Soles, C. L.; Lenhart, J. L.; Wu, W.-L.; Angelopoulos, M. In Polymers for Microelectronics and Nanoelectronics, ACS Symp Ser 874, 2004, p 86.

13. Wunnicke, O.; Hennig, A.; Grundke, K.; Stamm, M.; Czech, G. Proc SPIE 2002, 4690, 332–341.
14. Ishida, M.; Kobayashi, K.; Fujita, J.-I.; Ochiai, Y.; Yamamoto, H.; Tono, S. Jpn J Appl Phys 2002, 41, 4228–4232.
15. The data in this article and in the figures are presented along with the standard uncertainty (±) involved in the measurement. The uncertainty represents one standard deviation from the mean.
16. Lin, E. K.; Soles, C. L.; Goldfarb, D. L.; Trinque, B. C.; Burns, S. D.; Jones, R. L.; Lenhart, J. L.; Angelopoulos, M.; Willson, C. G.; Satija, S. K.; Wu, W.-L. Science 2002, 297, 372–375.
17. Certain commercial equipment and materials are identified in this article to specify adequately the experimental procedure. In no case does such specification imply recommendation by the National Institutes of Standards and Technology, nor does it imply that the material or equipment specified is necessarily the best available for this purpose.
18. Lenhart, J. L.; Jones, R. L.; Lin, E. K.; Soles, C. L.; Wu, W.-L.; Goldfarb, D. L.; Angelopoulos, M. J Vac Sci B 2002, 20, 706–709.
19. Hinsberg, W. D.; Houle, F. A.; Sanchez, M. I.; Walraff, G. M. IBM J Res Dev 2001, 45, 667–682.